Proceedings World Geothermal Congress 2015
Melbourne, Australia, 19-25 April 2015

Influences on the Barite Precipitation from Geothermal Brines

Tina Canic, Sabine Baur, Thomas Bergfeldt and Dietmar Kuhn

Karlsruhe Institute of Technology (KIT-IKET), Hermann-von-Helmholtz-Platz 1, D-76344 Eggenstein-Leopoldshafen, Germany

E-mail: tina.canic@kit.edu

Keywords: Precipitation, scaling, barite, barium sulfate, kinetics, shear rate influence

ABSTRACT

Barite is one of the toughest scaling minerals in geothermal power plants all over the world using saline wells of deep sedimentary basins. It is highly insoluble, can incorporate radioactive isotopes, and its scaling persists on the walls causing constriction or even blockage of system components. Removing the scales is only possible by mechanical means. To help preventing barite scale formation a profound understanding of precipitation and scaling processes is necessary.

This study focusses on the parameters that influence the velocity of barite precipitation. These include:

- Supersaturation
- Overall salt concentration
- Shear rate (as a measure for the flow conditions)
- Contact surface
- Crystallization nuclei
- Molar ratio $n(Ba^{2+})/n(SO_4^{2-})$

To determine the barite precipitation rate at different shear rates, a special annular gap apparatus has been developed. This apparatus ensures constant shear rates in the solution. Overall salt concentration was varied by using three model geothermal brines. These are solutions with different salt concentrations. Each resembles the water composition of one of three European geothermal sites (total dissolved salt between 90 and 265 g/L). The molar ratio of barium ions and sulfate ions was varied from 1:1 up to a twelvefold sulfate excess. Furthermore, the influence of different contact surfaces like glass and polymethyl methylacrylate (PMMA) as well as crystallization nuclei have been examined.

Experiments were carried out at room temperature. Supersaturation was attained by adding barium and sulfate ions separately in the form of barium chloride ($BaCl_2$) and sodium sulfate (Na_2SO_4) solutions in the necessary excessive amounts. To measure the precipitation progress, the remaining barium ions were analyzed by probe sampling.

Barite precipitation rate rises with higher shear rates. This influence is more distinctive when regarding brines with lower overall salt concentration. At these concentrations, barite precipitates more rapidly than at higher salt concentrations. A high sulfate excess as well as a large supersaturation accelerate precipitation. Precipitation is slower when using glass instead of PMMA. When adding crystal nuclei before starting, precipitation is unexpectedly fast.

1. INTRODUCTION

1.1 Precipitation issues

Precipitation and scaling of minerals are serious issues in geothermal plants. At many sites all over the world these phenomena have been reported, see e.g. Akaku (1990), Jones et al. (1996), and Lindal and Kristmannsdóttir (1989). The most frequent types of scales observed are carbonates ($CaCO_3$), sulfates ($CaSO_4$, $BaSO_4$, $SrSO_4$), silica (SiO_2), and sulfides (FeS, PbS, CuS) (Gardner and Nancollas, 1983; Stober and Bucher, 2012). These scales cause constriction or even blockage in feed pipes and other system components. When formed in heat exchangers, they reduce the heat transfer and thus the whole efficiency of the system (Bott, 1995). Last but not least, precipitated crystals can be reinjected and can clog the pores of the reservoir. This can result in the need for higher reinjection pressure.

1.2 Baryte

This study focusses on barite (barium sulfate, $BaSO_4$) precipitation for several reasons. First, barite is found in many geologic environments and many occurrences are hydrothermal in origin (Blount, 1977; Strübel, 1967). Several geothermal waters, e.g. in Nevada (Breit et al., 2010), Texas (Fisher, 1995) and the Salton Sea (McLin et al., 2006) have a high potential for barite precipitation. Especially low enthalpy geothermal power plants using waters from deep sedimentary basins find barite scales downstream of the power plant (Mergner et al., 2012; Scheiber et al., 2012).

Furthermore, with its solubility of ca. 1.4 mg/L, barite is an extremely insoluble salt (Monnin and Galinier, 1988; Templeton, 1960). The petroleum industry speaks of a "particularly intractable scaling agent" (Christy and Putnis, 1993). Barite scaling can form already in the wellbore or above the ground. In both cases, it requires mechanical removal whereas chemical means like the addition of acids do not suffice (Christy and Putnis, 1993; He et al., 1995). Therefore, barite is a high risk for the operational reliability of geothermal plants (Degering and Köhler, 2009; Degering et al., 2011).

Consequently, a profound understanding of the processes and parameters that influence barite formation in geothermal plants can help towards preventing their formation in geothermal power plants, thus improving system efficiency and running costs.

1.3 Precipitation influencing parameters

1.3.1 Supersaturation

Barite ($BaSO_4$) precipitates from a solution with excess amounts of barium cations Ba^{2+} and sulfate anions SO_4^{2-} as follows:

$$Ba^{2+} + SO_4^{2-} \rightleftharpoons BaSO_4 \downarrow \quad (1)$$

The measure for the excess amount, i.e. the supersaturation, is the saturation index *SI*:

$$SI = \lg \frac{a(Ba^{2+})_{actual} \cdot a(SO_4^{2-})_{actual}}{a(Ba^{2+})_{equil} \cdot a(SO_4^{2-})_{equil}} \quad (2)$$

where $a(Ba^{2+})_{actual}$ and $a(SO_4^{2-})_{actual}$ are the actual activities of the barium and sulfate ions and $a(Ba^{2+})_{equil}$ and $a(SO_4^{2-})_{equil}$ are the activities of the barium and sulfate ions at equilibrium. The higher the SI the more barium sulfate can precipitate. In this paper, saturation indices have been calculated with PHREEQC, version 3.1.2. (Parkhurst and Appelo, 2013).

In geothermal plants, the brine saturated with minerals is cooled down in the heat exchanger. Typical temperature changes range from ~ 123 – 175 °C to 60 – 70 °C (Mergner et al., 2012). With decreasing temperature, solubility of barite decreases. Thus, the geothermal brine becomes supersaturated in barite. The experiments in this study were performed at room temperature. Supersaturation was attained by adding barium chloride ($BaCl_2$) and sodium sulfate (Na_2SO_4) solutions in the necessary excessive amounts.

1.3.2 Overall salt concentration

When adding a barium chloride solution to a sodium sulfate solution, such that the resulting solution is supersaturated in barite, immediately a white barite precipitate can be observed. Yet, performing this experiment in a sulfate solution with e.g. 200 g/L dissolved sodium chloride, the occurrence of the white precipitate is delayed. The same happens in highly saline geothermal brines. In these waters, barite does not precipitate immediately despite being thermodynamically supersaturated. In fact, it has been shown that precipitation can be kinetically inhibited (Kaufmann-Knoke, 1992; Kühn et al., 1997).

1.3.3 Shear

Experiments have indicated that solution movement influences the barite precipitation rate (in water: Fitchett and Tarbell (1990), in brines: Seibt (2008)). The influence of solution movement on precipitation can be determined using well-defined fluid shear rates.

Fluids are subject to shear when neighboring fluid layers at a distance (r) move with different velocities (u) (Figure 1). The relevant physical quantity is the shear stress. For Newtonian fluids, shear stress is proportional to the shear rate:

$$\tau = \mu \frac{du}{dr} \quad (3)$$

where τ, μ and du/dr are the shear stress, the dynamic viscosity and the shear rate, respectively. To examine dependencies between precipitation rates and shear rates, it is important to keep the shear rate constant throughout the fluid. The ideal case would be a plane gap (Figure 1, left), where the shear rate du/dr is constant throughout the entire gap. This is called "plane Couette flow"(Yamaguchi, 2008). For an experimental setup (see Chapter 2.2) the plane gap can be approximated by an annular gap (Figure 1, right), the plane plates are then replaced by two coaxially arranged cylindrical vessels. Due to the curvature of the vessels, shear is not constant along the whole gap but depends on the radius r (Yamaguchi, 2008) as indicated in Figure 1, right.

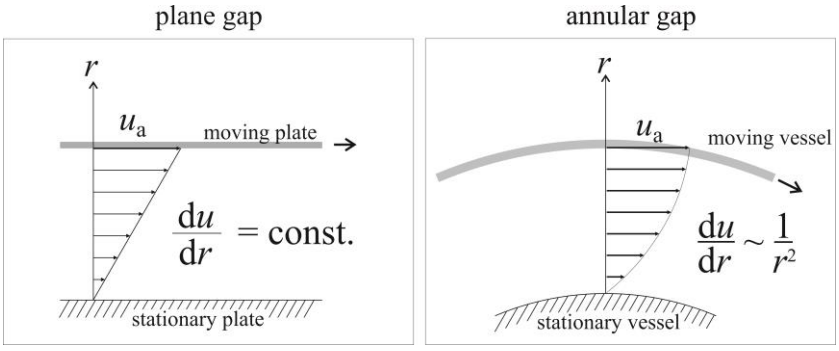

Figure 1: Plane Couette flow in a plane gap (left) and circular Couette flow in an annular gap (right). u_a: velocity of the moving plate/vessel, r: distance between the moving and the stationary plate/vessel.

The larger the ratio between the vessel radius and the width of the annular gap, the more the experimental setup approaches the ideal setup of a plane gap.

1.3.4 Contact surface and crystallization nuclei

The first step of precipitation is nucleation, either in a homogenous manner with crystallization nuclei forming in the solution or in a heterogeneous manner at the vessel surface. Once a critical amount of crystallization nuclei has been formed, crystal growth will

proceed more rapidly on the nuclei surface. Therefore, in this study the precipitation rate has been studied in vessels with different surfaces (glass, polymethyl methylacrylate (PMMA), steel) as well as within suspensions of barite crystals as nuclei.

1.3.5 Molar ratio $n(Ba^{2+})/n(SO_4^{2-})$

Aoun et al. (1996) and Kowacz et al. (2007) have shown in experiments in water, that – at the same supersaturation – a molar balance between cations and anions does not result in the fastest crystallization rate. Analyses of geothermal brines from the Upper Rhine Graben usually show sulfate excess (Scheiber et al., 2012), whereas brines from the North German Basin have molar ratios up to stoichiometric (Seibt and Wolfgramm, 2003). Therefore, in this study the precipitation of barite has been studied with molar ratios $n(Ba^{2+})/n(SO_4^{2-})$ from 1 to 1/12.

2. EXPERIMENTAL SETUP AND ANALYTICS

2.1 Dimensioning

When establishing dimensions for the experimental setup, two conflicting factors have to be reconciled. On the one hand, as indicated in Chapter 1.3.3, the radii of the vessels should be as large as possible and the annular gap as small as possible; on the other hand, the setup must be technically feasible and manageable. We chose an annular gap width of $r_a - r_i = 10$ mm, where r_a and r_i are the inner radius of the outer vessel and the outer radius of the inner vessel, respectively (see Figure 2). This offers sufficient space for filling and emptying the annular gap with fluid, as well as for taking fluid samples. With this annular gap width, the radii of the vessels were determined so that the shear stress within the annular gap deviated by no more than 5% from the shear stress within a flat gap of the same width. The resultant outer annular gap diameter was $2r_a = 400$ mm.

Evaporation was minimized by ensuring that the surface of the fluid inside the annular gap was as small as possible in relation to the total volume. Our calculations resulted in a fill capacity of about 5 L and a vessel height of at least 400 mm.

2.2 Annular gap apparatus

Figure 2 shows a schematic diagram and photo of the annular gap apparatus. Two polymethyl methacrylate (PMMA) tubes (drawn in yellow and orange) were mounted with an annular gap of 10 mm on two pivot-mounted circular base plates and sealed. The lower base plate, on which the outer tube is mounted, is connected to a motor. This arrangement allowed different constant rotation velocities and thus shear rates to be applied.

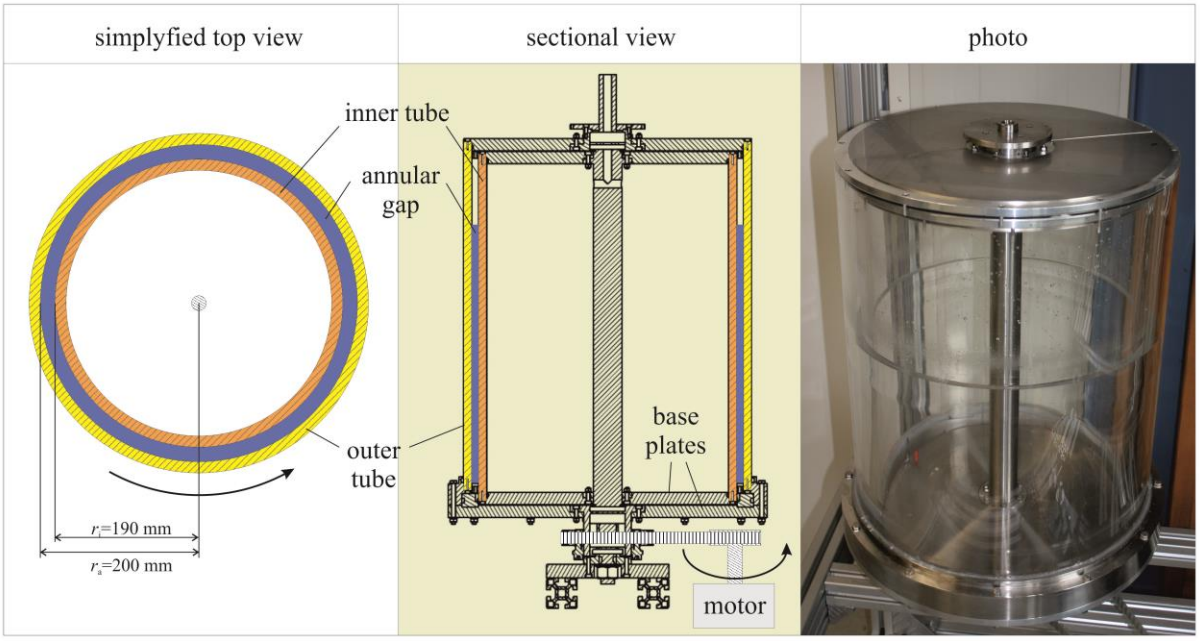

Figure 2: Schematic drawing (top and sectional view) and photo of the annular gap apparatus setup

2.3 Model brines

The chemical composition of the highly saline geothermal brines is very complex. For the experiments in this project, representative model brines were prepared based on the investigations of Seibt (2008 and 2013) (see Table 1).

	Type North German Basin (NGB)	**Type Upper Rhine Graben, I (URG-I)**	**Type Upper Rhine Graben, II (URG-II)**
NaCl	104 g/L (1.774 mol/L)	77.1 g/L (1.320 mol/L)	70.6 g/L (1.208 mol/L)
$CaCl_2$	161 g/L (1.449 mol/L)	24.8 g/L (0.224 mol/L)	21.9 g/L (0.197 mol/L)
TDS	264 g/L	106 g/L	92.5 g/L

Table 1: Composition of the model brines (TDS: total dissolved salt)

2.4 Experiments

The experiments were carried out in the annular gap apparatus and in vessels of glass and PMMA. First, the vessel or the annular gap was filled with a defined quantity of model brine (NaCl: Sodium chloride for analysis EMSURE®, Merck KGaA; $CaCl_2$:

Calcium chloride dihydrate for analysis EMSURE®, Merck KGaA). Then, a specific amount of Na_2SO_4 (Sodium sulfate anhydrous for analysis EMSURE®, Merck KGaA), either as salt or as stock solution, was added. At last, the addition of the appropriate volume of a $BaCl_2$ (Barium chloride dihydrate for analysis EMSURE®, Merck KGaA) stock solution determined the start of the reaction. The experimental conditions are listed in Table 2. For the experiments K001 to K003, 400 g of $BaSO_4$ (Barium sulfate suitable for use as excipient EMPROVE®, Merck KGaA) were suspended in 1 L of model brine before adding $BaCl_2$ and Na_2SO_4 stock solutions.

Exp't # (model brine)	$\beta_0(Ba^{2+})$ [mg/L]	$c_0(Ba^{2+})$ [mmol/L]	$\beta_0(SO_4^{2-})$ [mg/L]	$c_0(SO_4^{2-})$ [mmol/L]	$n(Ba^{2+})/n(SO_4^{2-})$	*SI*	Rotation velocity	Vessel
2 (NGB)	135.4	0.986	94.7	0.986	1/1	1.48	2/min	annular gap
3 (NGB)	135.5	0.987	94.8	0.987	1/1	1.48	10/min	annular gap
9 (URG-I)	69.6	0.507	300.3	3.126	1/6.16	1.96	0/min	annular gap
10 (URG-I)	69.7	0.507	300.3	3.126	1/6.16	1.96	2/min	annular gap
12 (URG-I)	69.6	0.507	300.3	3.126	1/6.16	1.96	40/min	annular gap
14 (URG-I)	69.7	0.507	300.3	3.126	1/6.16	1.96	0/min	annular gap
15 (URG-I)	69.7	0.507	300.3	3.126	1/6.16	1.96	2/min	annular gap
17 (URG-I)	69.7	0.507	300.3	3.126	1/6.16	1.96	40/min	annular gap
19 (NDB)	134.6	0.980	94.2	0.980	1/1	1.47	0/min	annular gap
20 (NDB)	134.6	0.980	94.2	0.980	1/1	1.47	10/min	annular gap
25 (URG-I)	166.3	1.211	116.3	1.211	1/1	1.93	40/min	annular gap
26 (URG-I)	166.3	1.211	116.3	1.211	1/1	1.93	stirrer	PMMA-vessel
27 (URG-I)	166.3	1.211	116.3	1.211	1/1	1.93	0/min	PMMA-vessel
28 (URG-I)	166.3	1.211	116.3	1.211	1/1	1.93	0/min	glass vessel
29 (URG-I)	166.3	1.211	116.3	1.211	1/1	1.93	stirrer	glass vessel
30 (URG-I)	171.0	1.245	119.6	1.245	1/1	1.95	0/min	annular gap
42 (URG-I)	48.3	0.352	422.7	4.400	1/12.5	1.95	stirrer	glass vessel
45 (URG-I)	48.3	0.352	422.7	4.400	1/12.5	1.95	0/min	annular gap
60 (URG-II)	68.3	0.498	298.9	3.111	1/6.25	1.99	0/min	annular gap
61 (URG-II)	68.3	0.498	298.9	3.111	1/6.25	1.99	2/min	annular gap
62 (URG-II)	68.3	0.498	298.9	3.111	1/6.25	1.99	10/min	annular gap
63 (URG-II)	68.3	0.498	298.9	3.111	1/6.25	1.99	40/min	annular gap
66 (URG-II)	48.3	0.352	422.7	4.400	1/12.5	1.99	0/min	annular gap
67 (URG-II)	48.3	0.352	422.7	4.400	1/12.5	1.99	2/min	annular gap
69 (URG-II)	48.3	0.352	422.7	4.400	1/12.5	1.99	40/min	annular gap
K001 (URG-I)	17.4	0.126	75.9	0.791	1/6.25	1.95	stirrer	glass vessel
K002 (URG-I)	68.4	0.498	298.9	3.111	1/6.25	1.95	stirrer	glass vessel
K003 (URG-I)	97.7	0.711	427.1	4.446	1/6.25	2.26	stirrer	glass vessel
UE02 (URG-I)	17.4	0.126	75.9	0.791	1/6.25	0.76	stirrer	glass vessel
UE04 (URG-I)	53.7	0.391	234.7	2.443	1/6.25	1.74	stirrer	glass vessel
UE06 (URG-I)	68.4	0.498	298.9	3.111	1/6.25	1.95	stirrer	glass vessel
UE08 (URG-I)	97.7	0.711	427.1	4.446	1/6.25	2.26	stirrer	glass vessel
UE10 (NDB)	43.4	0.316	30.4	0.316	1/1	0.49	stirrer	glass vessel
UE12 (NDB)	134.2	0.977	93.8	0.977	1/1	1.46	stirrer	glass vessel
UE14 (NDB)	170.8	1.244	119.5	1.244	1/1	1.67	stirrer	glass vessel
UE16 (NDB)	244.1	1.778	170.8	1.778	1/1	1.98	stirrer	glass vessel
UE30 (URG-I)	97.2	0.708	68.0	0.708	1/1	1.46	stirrer	glass vessel
UE31 (URG-I)	97.2	0.708	68.0	0.708	1/1	1.46	0/min	glass vessel
UE32 (URG-I)	172.9	1.259	120.9	1.259	1/1	1.96	stirrer	glass vessel
UE33 (URG-I)	172.9	1.259	120.9	1.259	1/1	1.96	0/min	glass vessel
UE34 (NDB)	134.2	0.977	93.9	0.977	1/1	1.47	stirrer	glass vessel
UE35 (NDB)	134.2	0.977	93.9	0.977	1/1	1.47	0/min	glass vessel
UE36 (NDB)	238.6	1.738	166.9	1.738	1/1	1.96	stirrer	glass vessel
UE37 (NDB)	238.6	1.738	166.9	1.738	1/1	1.96	0/min	glass vessel

Table 2: Experimental conditions (β: mass concentration, c: molar concentration, index 0 indicates start of reaction, n: amount of substance, *SI*: saturation index)

At pre-determined times the vessel's rotation was briefly stopped and a sample was taken by means of a probe attached to a syringe. The samples were filtered through a nylon syringe filter (diameter: 15 mm, pore size: 0.2 µm) and diluted by a factor of 1:100 (URG) or 1:200 (NDB), respectively. Concentrated nitric acid was added to prevent blockage of the nozzles of the analytical instrument by salt precipitation. The samples were then analyzed as described in Section 2.5.

2.5 Measuring reaction progress

During the experiments (see Section 2.4), barite ($BaSO_4$) is formed according to Equation (1) (see Section 1.3.1). The progress of the reaction is measured via determining the concentration of barium ions remaining in the solution by probe sampling. This concentration decreases in the same amount as the concentration of precipitated barite rises.

Barium concentrations were determined by inductively coupled plasma optical emission spectrometry (ICP-OES). The detection limit of ICP-OES is at 1 µg/L barium, therefore it is well-suited for the detection of barium in saline solutions. Since the experimental solution must be diluted by a factor of 1:100 (URG) or 1:200 (NGB) because of the high initial salt concentration, the

detection limit for barium in the experimental solution itself was 0.1 mg/L or 0.2 mg/L, depending on the dilution factor. This is well below the solubility of barium from barium sulfate in water, which at 25 °C is about 1.4 mg/L (Monnin and Galinier, 1988; Templeton, 1960). Barium was measured at the two barium-specific wavelengths 455.403 nm and 493.408 nm with a PerkinElmer OPTIMA 4300 DV ICP-OES.

2.6 Error

To determine the reliability of the measured data repeat experiments were carried out. With these experiments, the measurement error has been determined to approximately 10%.

3. RESULTS AND DISCUSSION

3.1 Supersaturation

Figure 3 shows barium ion mass concentrations, normalized to the initial concentration, versus time at different saturation indices between $SI = 0.49$ and $SI = 2.26$. The model brines used were URG-I with 6.25-fold sulfate excess (left) and NDB with stoichiometric ratio $n(Ba^{2+})/n(SO_4^{2-})$ (right).

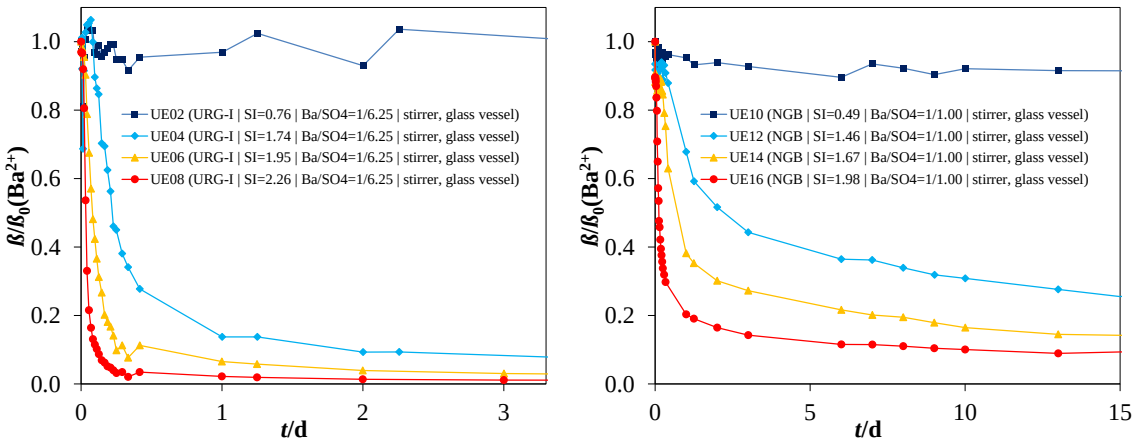

Figure 3: Barium ion mass concentration β (normalized to the initial concentration β_0) versus time at four different saturation indices *SI* in URG-I model brine with 6.25-fold sulfate excess (left) and in NGB model brine (right).

It can clearly be seen that in both model brines the decrease of the barium mass concentration and thus the formation of barite becomes faster with higher supersaturation. With the lowest SI, the barium mass concentration remains nearly constant. Even after 15 days (not shown in the left figure) no significant decrease is observed.

These observations correspond quite well with the experiments of Kühn et al. (1997), who found that barite precipitation of thermodynamically supersaturated barite solutions is inhibited at low supersaturations.

3.2 Overall salt concentration

Figure 4 compares two model brines at two different supersaturations. At both supersaturations, the decrease in barium ion mass concentration is faster in the URG-I model brine with lower overall salt concentration. This suggests lower barite precipitation velocities with rising overall salt solution. The difference in precipitation velocities is more distinct at the lower supersaturation (dotted lines).

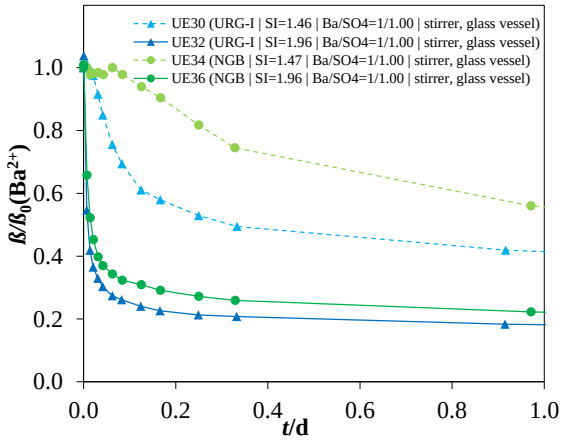

Figure 4: Barium ion mass concentration β (normalized to the initial concentration β_0) versus time *t* at different saturation indices *SI* and two different model brines (URG-I and NDB). Dotted lines represent the lower *SI* (1.47), solid lines the higher *SI* (1.96). Triangles represent the URG-I model brine, circles the NGB model brine.

This dependency corresponds quite well with the findings of Jones et al. (2004). They studied barite precipitation in the presence of calcium ions, though in an order of magnitude lower than in this paper and with only one initial barium concentration. They suggest that the slower precipitation with rising calcium ion concentration is a result of the higher solubility of barite and thus a lower supersaturation. The experiments presented here show, however, that even at the same supersaturation, barite precipitates slower when the overall salt concentration is higher. A possible explanation for that might be the suggestion of Hennessy and Graham (2002), that foreign ions act as a nucleation inhibitor. This effect seems to be more pronounced at lower supersaturation.

3.3 Shear

Figure 5 shows the results of experiments in glass vessels, stirred and unstirred, in URG-I (left) and NGB (right) model brine at two different supersaturations. In the URG-I model brine, the unstirred experiments (dotted lines) show a much slower decrease in barium concentration than the corresponding stirred experiments (solid line). In the NGB water, the difference between stirred and unstirred experiments is not significant.

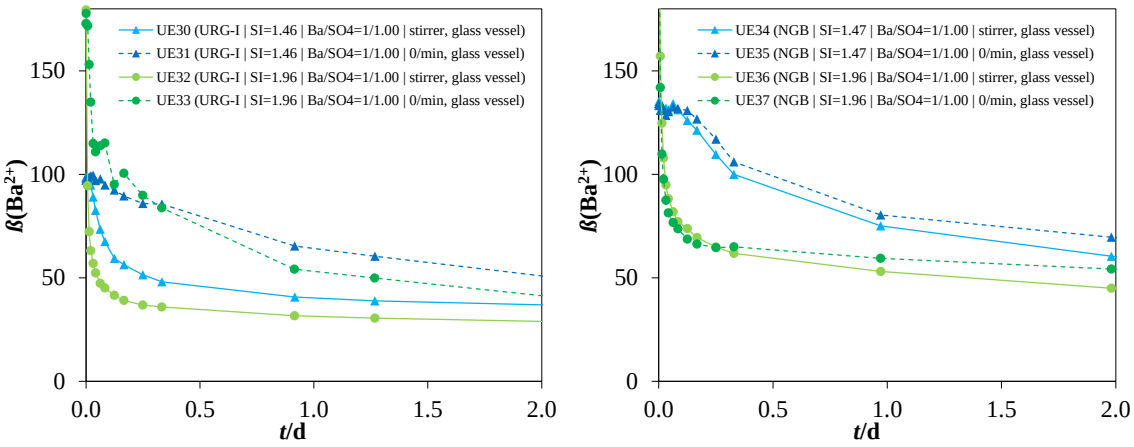

Figure 5: Barium ion mass concentration *β* versus time *t* in stirred (solid line) and unstirred (dotted line) URG-I (left) and NGB (right) model brine.

In the stirred experiments, the shear rate is not constant throughout the solution, so similar experiments were carried out in the annular gap apparatus with constant shear rates (see Chapter 1.3.3), given in vessel revolutions per minute. Figure 6 shows the results of the annular gap experiments at given shear rates in three different model brines.

In the URG-I model brine the influence of the shear rate is distinct, the precipitation is slow at 0/min, faster at 2/min and fastest at 40/min. Precipitation rate at 40/min shows the same fast decrease as in stirred experiments (see Figure 7), therefore this is considered as "maximum shear". The URG-II model brine contains 15 g/L less salt than the URG-I model brine (see Table 1). Here, too, the differences at different shear rates can clearly be seen, though there is no significant change between 2/min and 10/min. In the NGB model brine there is no significant difference between the three shear rates of 0/min, 2/min and 10/min.

In the URG model brines, where barite precipitation is generally faster than in the more saline NDB model brine, transport processes seem to be the limiting factor of the reaction. In the NDB model brine, the precipitation is so slow that even at 0/min transport processes seem to be fast enough. Fitchett and Tarbell (1990) have studied the influence of mixing on barite precipitation rates in pure water and have found, that the barite growth rate increases with higher mixing speed. They proposed mass transfer limited particle growth, too.

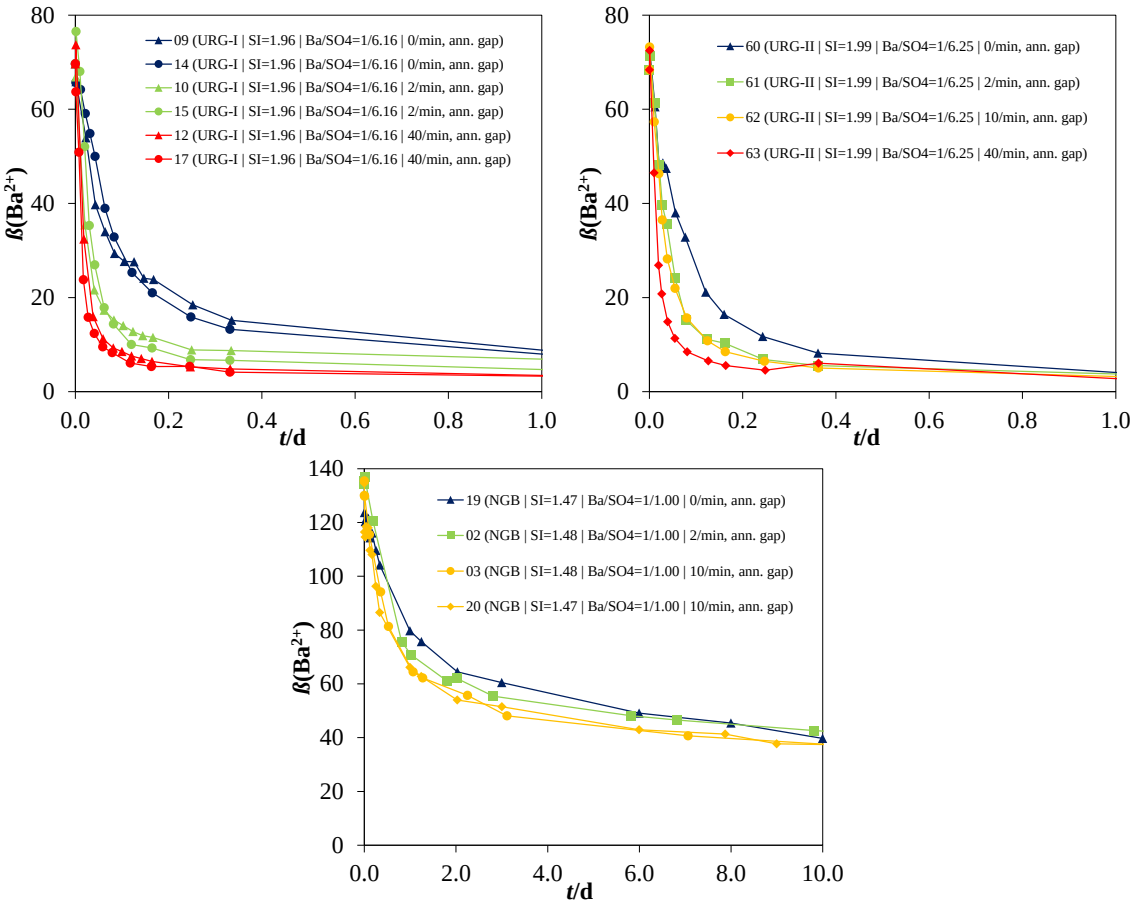

Figure 6: Barite ion mass concentration β versus time t in the annular gap apparatus at different shear rates with URG-I (top left), URG-II (top right) and NGB (bottom) model brine.

3.4 Contact surface and crystallization nuclei

The influence of different contact surfaces has been investigated by comparing the experiments in the annular gap, where the liquid is in contact with PMMA, steel and sealing material, with experiments in glass and PMMA vessels. For all experiments, the supersaturation was the same, Ba^{2+} and SO_4^{2-} were added stoichiometrically. Figure 7 shows the results for the unstirred experiments and at maximum stirring speed.

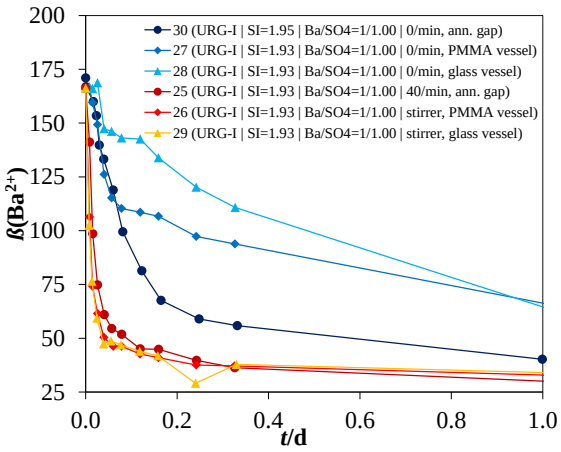

Figure 7: Barite ion mass concentration β versus time t in the annular gap, PMMA vessel and glass vessel at 0/min and maximum shear.

Differences can be seen in the unstirred experiments where the slowest reaction is the one in the glass vessel. The reaction in the PMMA vessel is faster, in the annular gap fastest. Regarding the stirred experiments, no significant difference can be seen between the three contact surface experiments. The barite precipitation in all the stirred experiments is faster than the fastest of the unstirred experiments. Therefore, stirring is the most effective accelerator for the reaction whereas surface effects are more effective in the unstirred solutions.

Glass surface is more polar than PMMA. It might therefore interact more strongly with the Ba^{2+} and SO_4^{2-} ions, thus leading to slower precipitation rates. In the annular gap, steel could have an accelerating effect on the crystallization. All these effects have to be studied further with other contact materials at equal surface to volume ratios.

Figure 8 shows the effect of barite crystals on the barite precipitation. For comparison, the two experiments UE02 and UE06 without barite crystals are shown, too.

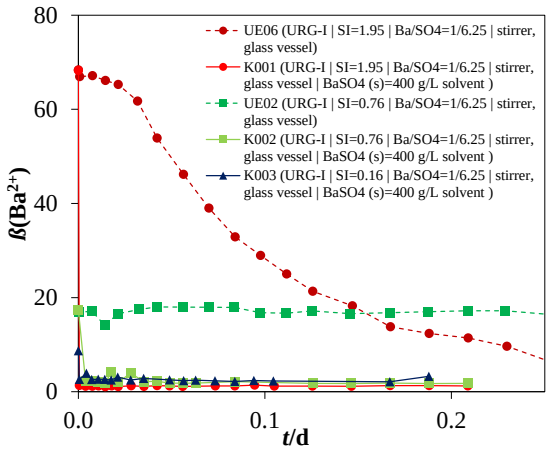

Figure 8: Barite ion mass concentration *β* versus time *t* in $BaSO_4$ suspension (K001 – K003). For comparison, experiments UE02 and UE06 without $BaSO_4$ suspension (dotted lines) were added to the graph.

Regarding K001 which corresponds to UE06, one can clearly see that, in the very short period of about 5 min between start of experiment and fist probing, the barium ion concentration of K001 drops to equilibrium concentration. Without crystals (UE06), this takes several hours.

At the lower saturation index of 0.76, in the experiment without barite crystals (UE02) barium ion concentration remains constant though the solution is supersaturated. With crystals (K002), concentration again immediately drops. This happens, too, even at the lowest supersaturation of *SI* = 0.16 (K003).

Barite crystallization nuclei immediately break down metastable supersaturated barite solutions even at a very low supersaturation of 0.16.

3.5 Molar ratio $n(Ba^{2+})/n(SO_4^{2-})$

Figure 9 shows experiments at different molar ratios $n(Ba^{2+})/n(SO_4^{2-})$ in the URG-I (left) and the URG-II (right) model brines. In the unstirred URG-I model brine, the barite precipitation becomes faster with rising sulfate excess. In the stirred solution, there is an increase in precipitation rate from stoichiometric to 6.16-fold sulfate excess, but little difference if not a slight decrease when about doubling the sulfate excess from 6.16 to 12.5.

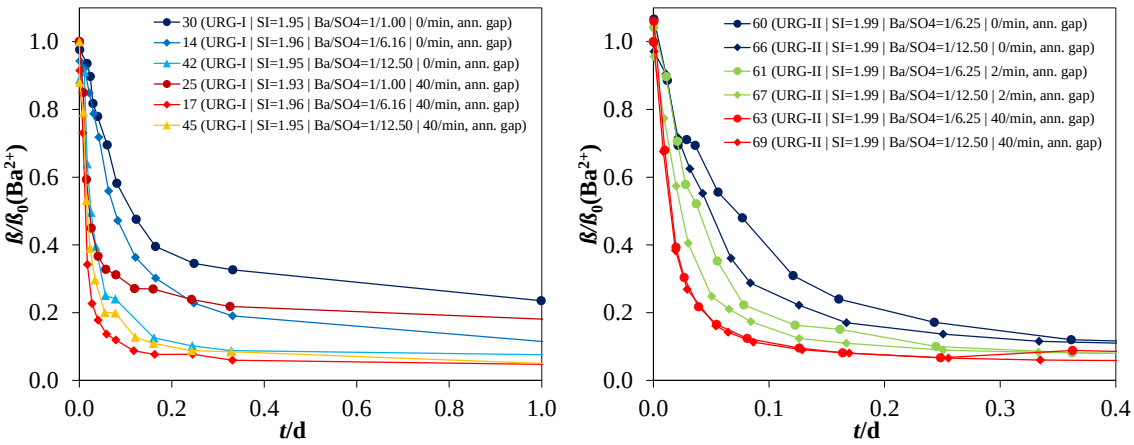

Figure 9: Barite ion mass concentration *β* versus time *t* at different molar ratios $n(Ba^{2+})/n(SO_4^{2-})$ in URG-I (left) and URG-II (right) model brine.

In the URG-II model brine (Figure 9, right) 6.25-fold and 12.5-fold sulfate excesses have been compared in the annular gap at different shear rates. Only at 0/min and 2/min, a difference in precipitation rate between 6.25 and 12.5-fold sulfate excess can be seen, the latter always being faster. At maximum speed of 40/min, here, too, no difference in precipitation rate between the two sulfate excesses can be seen.

Compared to stoichiometric ratio, sulfate excess accelerates barite precipitation in these saline brines. An excess in SO_4^{2-} ions enhances the probability that a Ba^{2+} ion gets in contact with them, thus forming barite. This is more important in the unstirred

solutions, where transport processes are slower than in the stirred solutions. Therefore, the effect in the unstirred solutions is more pronounced.

4. SUMMARY AND CONCLUSION

In this study, the influence of different parameters on the velocity of barite precipitation has been examined. Barite precipitation rate rises

- with rising supersaturation.
  Supersaturation is one of the driving forces of precipitation. The higher the supersaturation, the more barite can precipitate. With higher supersaturation, the concentrations of Ba^{2+} and SO_4^{2-} ions rise and thus the probability that a Ba^{2+} finds a SO_4^{2-} ion forming $BaSO_4$.

- with lower overall salt concentration.
  A high overall salt concentration enhances the potential for ion-ion interactions. They inhibit the fast combination of the two barite forming ions Ba^{2+} and SO_4^{2-}.

- with higher shear rate.
  A higher shear rate accelerates transport processes.

- extremely when barite particles as crystallization nuclei are provided.
  Barite crystals present a large surface which takes up Ba^{2+} and SO_4^{2-} ions separately without need of nucleation. Thus, the slow nucleation process is skipped and crystallization becomes very fast.

- when sulfate is added in excess.
  An excess in sulfate ions enhances the probability, that a Ba^{2+} ion gets in contact with a SO_4^{2-} ion, forming $BaSO_4$.

Furthermore, there are interdependencies between the above parameters. At higher shear rates, some other influences become smaller. When regarding different contact surfaces, a significant difference can only be seen without shear (Figure 7). A similar effect can be observed when regarding the accelerating effect of sulfate excess (Figure 9). Here, too, the acceleration is much more pronounced at smaller shear rates. This indicates a very strong influence of mixing on the barite precipitation.

The overall salt concentration affects other influencing parameters. In less saline brines, the accelerating effect of the shear rate on the barite precipitation rate is much more pronounced. This suggests, that in highly saline brines the inhibiting ion-ion interactions are stronger than the accelerating mixing effect at higher shear rates. At lower supersaturation, the decelerating effect of the high overall salt content is more distinct. As lower saturation itself leads to slower precipitation, high salt concentration enhances this effect.

REFERENCES

Akaku, K.: Geochemical study on mineral precipitation from geothermal waters at the fushime field, Kyushu, Japan, *Geothermics*, **19** (1990) 455-467.

Aoun, M., Plasari, E., David, R., Villermaux, J.: Are barium sulphate kinetics sufficiently known for testing precipitation reactor models?, *Chemical Engineering Science*, **51** (1996) 2449-2458.

Blount, C.W.: Barite solubilities and thermodynamic quantities up to 300 °C and 1400 bars, *Am Mineral*, **62** (1977) 942-957.

Bott, T.R.: *Fouling of heat exchangers*, ELSEVIER, Amsterdam, 1995.

Breit, G.N., Hunt, A.G., Wolf, R.E., Koenig, A.E., Fifarek, R.H., Coolbaugh, M.F.: *Are modern geothermal waters in northwest Nevada forming epithermal gold deposits?*, in: R. Steininger, B. Pennell (Eds.), Geological Society of Nevada Symposium 2010: Great Basin Evolution and Metallogeny, Reno, Nevada, 2010, 833-844.

Christy, A.G., Putnis, A.: The kinetics of barite dissolution and precipitation in water and sodium chloride brines at 44-85°C, *Geochimica et Cosmochimica Acta*, **57** (1993) 2161-2168.

Degering, D., Köhler, M.: *Natürliche Radionuklide in Anlagen der tiefen Geothermie*, Der Geothermiekongress 2009, Geothermische Vereinigung, Bundesverband Geothermie e.V., Bochum, 2009.

Degering, D., Köhler, M., Hielscher, M.: Vorkommen und Verhalten natürlicher Radionuklide im Aquifer, im Fluid und in den Ablagerungen der Geothermieanlage Neustadt-Glewe, *Zeitschrift fur Geologische Wissenschaften*, **39** (2011) 275-290.

Fisher, R.S.: Naturally occurring radioactive materials (NORM) in produced water and scale from Texas oil, gas, and geothermal wells: geographic, geologic, and geochemical controls, *Geological circular (University of Texas at Austin. Bureau of Economic Geology)* Volume 95-3, University of Texas at Austin. Bureau of Economic Geology, 1995.

Fitchett, D.E., Tarbell, J.M.: Effect of mixing on the precipitation of barium sulfate in an MSMPR reactor, *AIChE Journal*, **36** (1990) 511-522.

Gardner, G.L., Nancollas, G.H.: Crystal growth in aqueous solution at elevated temperatures. Barium sulfate growth kinetics, *The Journal of Physical Chemistry*, **87** (1983) 4699-4703.

He, S., Oddo, J.E., Tomson, M.B.: The nucleation kinetics of barium sulfate in NaCl solutions up to 6 m and 90°C, *Journal of Colloid and Interface Science*, **174** (1995) 319-326.

Hennessy, A.J.B., Graham, G.M.: The effect of additives on the co-crystallisation of calcium with barium sulphate, *Journal of Crystal Growth*, **237-239, Part 3** (2002) 2153-2159.

Jones, B., Renaut, R.W., Rosen, M.R.: High-temperature (>90°C) calcite precipitation at Waikite Hot Springs, North Island, New Zealand, *Journal of the Geological Society*, **153** (1996) 481-496.

Jones, F., Oliviera, A., Parkinson, G.M., Rohl, A.L., Stanley, A., Upson, T.: The effect of calcium ions on the precipitation of barium sulphate 1: calcium ions in the absence of organic additives, *Journal of Crystal Growth*, **262** (2004) 572-580.

Kaufmann-Knoke, R.: *Zur Problematik von Mineralausfällungen insbesondere von (Ba,Sr)SO_4-Mischkristallen bei der Erdölförderung*, Berichte - Reports, Geolog.-Paläont. Inst., Christian-Albrechts-Universität Kiel, Kiel, 1992, pp. 110.

Kowacz, M., Putnis, C.V., Putnis, A.: The effect of cation:anion ratio in solution on the mechanism of barite growth at constant supersaturation: Role of the desolvation process on the growth kinetics, *Geochimica et Cosmochimica Acta*, **71** (2007) 5168-5179.

Kühn, M., Frosch, G., Kölling, M., Kellner, T., Althaus, E., Schulz, H.D.: Experimentelle Untersuchungen zur Barytübersättigung einer Thermalsole, *Grundwasser*, **2** (1997) 111-117.

Lindal, B., Kristmannsdóttir, H.: The scaling properties of the effluent water from Kizildere power station, Turkey, and recommendation for a pilot plant in view of district heating applications, *Geothermics*, **18** (1989) 217-223.

McLin, K.S., Moore, J.N., Hulen, J., Bowman, J.R., Berard, B.: *Mineral characterization of scale deposits in injection wells; Coso and Salton Sea geothermal fields, CA*, Thirty-First Workshop on Geothermal Reservoir Engineering, Stanford University, Stanford, California, 2006.

Mergner, H., Eggeling, L., Kölbel, T., Münch, W., Genter, A.: Geothermische Stromerzeugung: Bruchsal und Soultz-sous-Forêts, *mining + geo*, (2012) 666-673.

Monnin, C., Galinier, C.: The solubility of celestite and barite in electrolyte solutions and natural waters at 25°C: A thermodynamic study, *Chemical Geology*, **71** (1988) 283-296.

Parkhurst, D.L., Appelo, C.A.J.: Description of input and examples for PHREEQC version 3 — A computer program for speciation, batch-reaction, one-dimensional transport, and inverse geochemical calculations, *U.S. Geological Survey Techniques and Methods*, chap. A43, book 6, 2013, pp. 497, http://pubs.usgs.gov/tm/06/a43/pdf/tm6-A43.pdf.

Scheiber, J., Nitschke, F., Seibt, A., Genter, A.: *Geochemical and mineralogical monitoring of the geothermal power plant in Soultz-sous-Forêts (France)*, Thirty-Seventh Workshop on Geothermal Reservoir Engineering, Stanford University, Stanford, California, USA, 2012, pp. 1033-1044.

Seibt, A.: *Abschlussbericht zum BMU-Vorhaben „Betrachtungen zu Lösungs- und Fällungsreaktionen und deren Einfluss auf den Kreislauf einer Geothermieanlage zur Stromerzeugung" (Förderkennzeichen: 0329951 F)*, 2008, http://edok01.tib.uni-hannover.de/edoks/e01fb09/607466502.pdf.

Seibt, A.: *Personal Communication*, 2013.

Seibt, A., Wolfgramm, M.: *Stimulation tests in a deep Rotliegend sandstone formation – Geochemical aspects*, IGC-2003 - International Geothermal Conference, Reykjavík, Iceland, 2003.

Stober, I., Bucher, K.: *Geothermie*, Springer, Heidelberg, 2012.

Strübel, G.: Zur Kenntnis und genetischen Bedeutung des Systems $BaSO_4$ - NaCl - H_2O, *Neues Jahrbuch Mineral. Monatsh.*, (1967) 223-234.

Templeton, C.C.: Solubility of barium sulfate in sodium chloride solutions from 25° to 95°C, *Journal of Chemical & Engineering Data*, **5** (1960) 514-516.

Yamaguchi, H.: *Engineering mechanics*, Springer, 2008.